

## **Supporting Information**

### **Viewing Human DNA Polymerase $\beta$ Faithfully and Unfaithfully Bypass an Oxidative Lesion by Time-Dependent Crystallography**

Rajan Vyas<sup>1</sup>, Andrew J. Reed<sup>1,2</sup>, E. John Tokarsky<sup>1,3</sup>, and Zucai Suo<sup>1,2,3,\*</sup>

<sup>1</sup>Department of Chemistry and Biochemistry, The Ohio State <sup>2</sup>Biochemistry and <sup>3</sup>Biophysics  
Programs, The Ohio State University, Columbus, OH 43210, USA

\*To whom correspondence should be addressed: Zucai Suo, Department of Chemistry and  
Biochemistry, The Ohio State University, Columbus, OH 43210, USA; Tel.: (614) 688-3706;  
Fax: (614) 292-6773; E-mail: suo.3@osu.edu

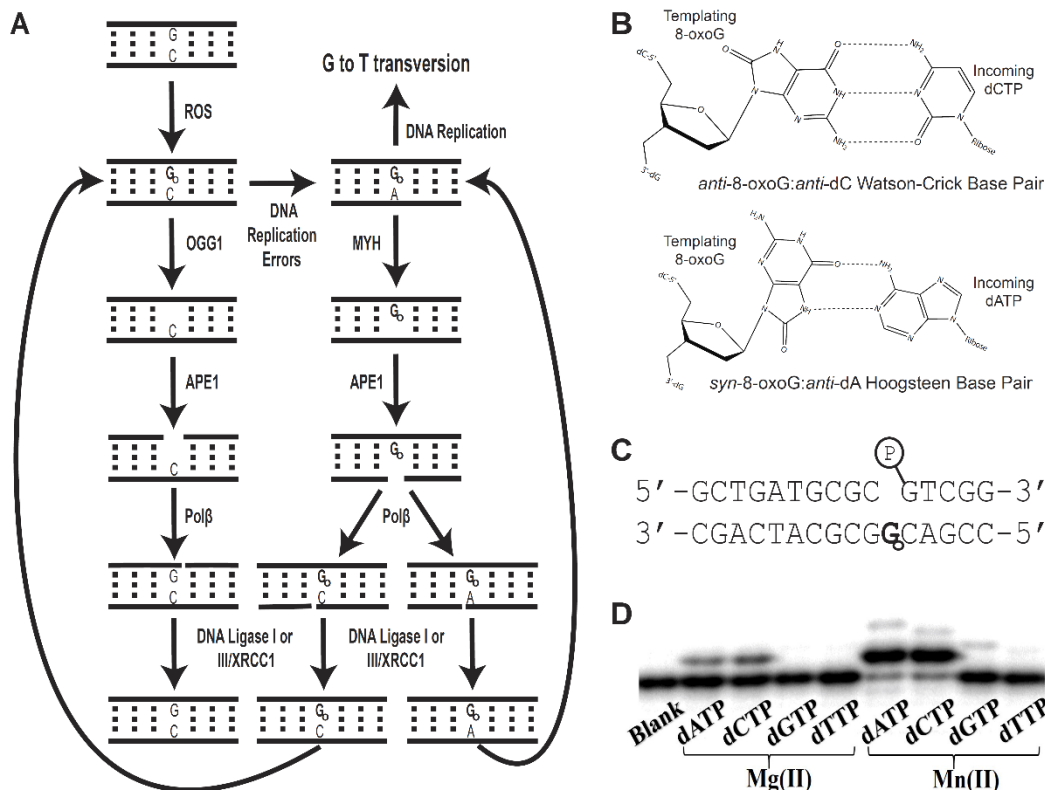


**Figure S1. 8-oxoG and Base Excision Repair (BER)** (A) Generation and repair of 8-oxoG by BER in eukaryotes is shown. Intracellular reactive oxygen species (ROS) damage genomic DNA and form various lesions including 8-oxoG ( $G_o$ ). Most *anti*-8-oxoG:*anti*-dC base pairs are repaired by removal of the damaged guanine base via an oxoguanine DNA glycosylase OGG1. The backbone of the resulting apurinic site is then cleaved by apurinic endonuclease 1 (APE1). DNA polymerase  $\beta$  (Pol $\beta$ ) then performs gap-filling synthesis and deoxyribose cleavage. Finally, DNA ligase I or III/XRCC1 complex ligates the nicked DNA substrate to complete BER. Any *anti*-8-oxoG:*anti*-dC pairs that go unrepaired may undergo erroneous DNA replication and result in *syn*-8-oxoG:*anti*-dA mispairs in genomic DNA. Repair of a *syn*-8-oxoG:*anti*-dA mispair begins with the removal of the undamaged adenine base via an adenine DNA glycosylase MYH. Subsequently, the apurinic site is processed by APE1, Pol $\beta$  and DNA ligase I or III/XRCC1 in BER. Notably, Pol $\beta$ -catalyzed gap-filling synthesis can result in either *syn*-8-oxoG:*anti*-dA mispairs or *anti*-8-oxoG:*anti*-dC correct pairs due to the dual coding potential of 8-oxoG. The *anti*-8-oxoG:*anti*-dC pairs can be repaired through the OGG1 branch of the BER pathway while the *syn*-8-oxoG:*anti*-dA pairs can reenter the MYH branch of the pathway. Alternatively, both base pairs could enter DNA replication where *syn*-8-oxoG:*anti*-dA base pairs would result in G to T transversion. (B) The *anti*-8-oxoG:*anti*-dCTP Watson-Crick base pair and the *syn*-8-oxoG:*anti*-dATP Hoogsteen base pair. (C) A single-nucleotide gapped DNA substrate (**8-oxoG-DNA**) for our crystallization and  $^{32}\text{P}$ -labeled primer extension assay. The downstream primer 5-mer was 5'-phosphorylated while the upstream primer 10-mer was not. The templating 8-oxoG is shown as  $G_o$ . (D) Gel image of the  $^{32}\text{P}$ -labeled primer extension assay. A preincubated solution of hPol $\beta$  (10 nM) and 5'-[ $^{32}\text{P}$ ]-labeled 8-oxoG-DNA (30 nM) was reacted with the indicated dNTP (100  $\mu\text{M}$ ) for 15 s in the presence of either  $\text{Mg}^{2+}$  (left lanes) or  $\text{Mn}^{2+}$  (right lanes) at 25  $^\circ\text{C}$  and then quenched with 0.37 M EDTA. "Blank" indicates no nucleotides added in the reaction.

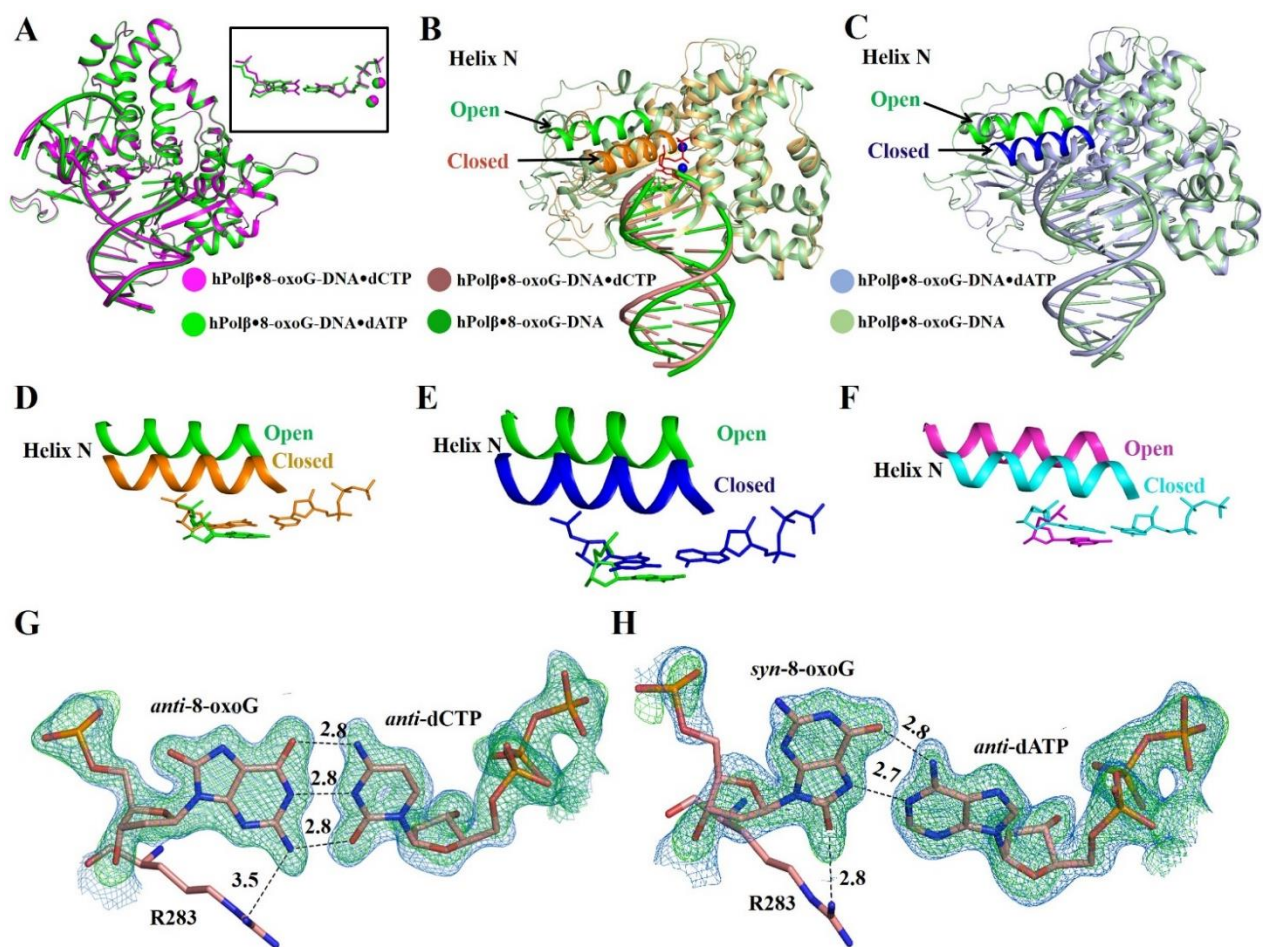


**Figure S2. Structural differences between various ternary and binary complexes and the binding conformations of 8-oxoG at the active site of hPolβ in the pre-catalytic ternary complex of hPolβ•8-oxoG-DNA•dCTP or hPolβ•8-oxoG-DNA•dATP.** (A) Superposition of the pre-catalytic ternary complexes of hPolβ•8-oxoG-DNA•dCTP and hPolβ•8-oxoG-DNA•dATP in the presence of Ca<sup>2+</sup>. The close-up view shows the overlaying of the nascent base pair and Ca<sup>2+</sup> ions at the A- and B-site. (B) Superposition of the binary structure of hPolβ•8-oxoG-DNA (3RJE) and the pre-catalytic ternary structure of hPolβ•8-oxoG-DNA•dCTP with Ca<sup>2+</sup>. (C) Superposition of the binary structure of hPolβ•8-oxoG-DNA (3RJE) and the pre-catalytic ternary structure of hPolβ•8-oxoG-DNA•dATP with Ca<sup>2+</sup>. In (B) and (C), Helix N is in the same but darker color relative to the rest of the corresponding structure. (D) Zoomed view of Helix N and the nascent base pair in (B). (E) Zoomed view of Helix N and the nascent base pair in (C). (F) Zoomed view of Helix N and the nascent base pair in the overlaid structures of the binary complex of hPolβ•undamaged DNA (magenta, 3ISB) and the ternary complex of hPolβ•undamaged DNA•dCTP (cyan, 4KLD). (G) The electron density map for the nascent *anti*-8-oxoG:*anti*-dCTP Watson-Crick base pair in the pre-catalytic ternary complex of hPolβ•8-oxoG-DNA•dCTP with Ca<sup>2+</sup>. (H) The electron density map for the nascent *syn*-8-oxoG:*anti*-dATP Hoogsteen base pair in the pre-catalytic ternary complex of hPolβ•8-oxoG-DNA•dATP with Ca<sup>2+</sup>. In (G) and (H), the 2F<sub>o</sub>-F<sub>c</sub> (blue) and F<sub>o</sub>-F<sub>c</sub> (green) maps were contoured at 1σ and 3σ, respectively.

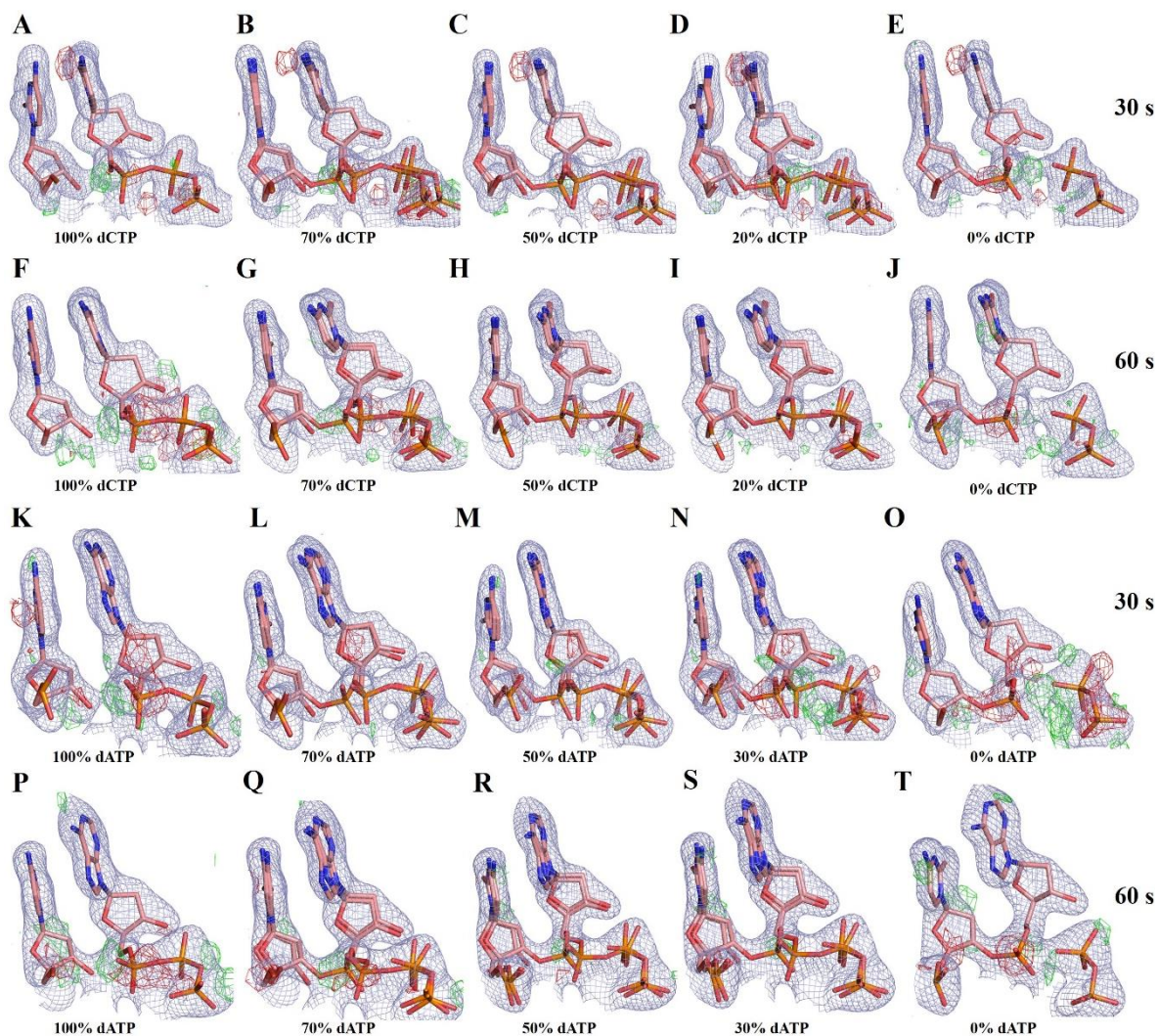


**Figure S3. Modeling of reactant-, reaction- and product-states during phosphodiester bond formation after 30 or 60 s of  $Mg^{2+}/Ca^{2+}$  ion-exchange.** The  $2F_o-F_c$  (light blue) maps contoured at  $1\sigma$  and the  $F_o-F_c$  omit maps contoured at either  $3\sigma$  (green) or  $-3\sigma$  (red) are presented for the primer 3'-terminal nucleotide, incoming nucleotide, incorporated nucleotide, and pyrophosphate. Only the occupancy of the reactant dCTP/dATP is listed below each structure. Strong positive (green) and negative (red) electron density blobs between the primer 3'-OH and the  $\alpha$ -phosphate group of dCTP/dCMP, between the  $\alpha$  and  $\beta$ -phosphate groups of dCTP, or between the phosphates of dCMP and pyrophosphate indicate unsatisfactory modeling, *e.g.* the modeling of the reactants at 100% (A), 70% (B), 20% (D), and 0% (E) occupancies for the 30 s structure and 100% (F), 70% (G), 50% (H), and 0% (J) occupancies for the 60 s structure. In contrast, the absence of any positive or negative electron density with the modeling of the reactants at 50% (C) and 20% (I) occupancies suggests satisfactory modeling for the 30 and 60 s structures, respectively. Similarly, for dATP incorporation, the modeling of the reactants at 100% (K), 50% (M), 30% (N), and 0% (O) occupancies for the 30 s structure and 100% (P), 70% (Q), 50% (R), and 0% (T) occupancies for the 60 s structure is unsatisfactory while the modeling of the reactants at 70% (L) and 30% (S) occupancies for the 30 and 60 s structures, respectively, is satisfactory.

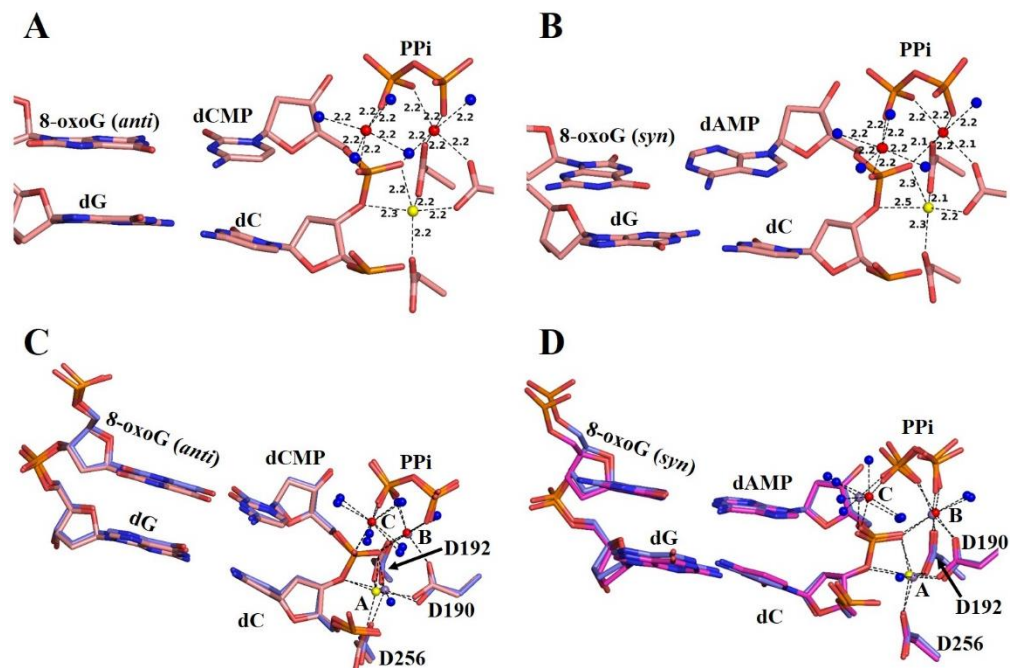


**Figure S4. Comparison of structures captured at different time points while incorporating either dCTP or dATP opposite 8-oxoG.** (A) Active site metal ion coordination distances for the dCTP incorporation product-state structure after  $\text{Mg}^{2+}/\text{Ca}^{2+}$  ion-exchange for 80 s. (B) Active site metal ion coordination distances for the dATP incorporation product-state structure after  $\text{Mg}^{2+}/\text{Ca}^{2+}$  ion-exchange for 80 s. (C) Superposition of the dCTP incorporation product-state structures after soaking crystals with  $\text{Mg}^{2+}$  for 80 s (salmon) and with  $\text{Mn}^{2+}$  for 35 s (blue). (D) Superposition of the dATP incorporation product-state structures after soaking crystals with  $\text{Mg}^{2+}$  for 80 s (pink) and with  $\text{Mn}^{2+}$  for 35 s (blue). From (A) to (D), active site metal ions, including  $\text{Mg}^{2+}$  (red),  $\text{Mn}^{2+}$  (purple) and  $\text{Na}^{+}$  (yellow), and water molecule ligands (blue) are represented as spheres. Note that the spheres for the metal ions are not representative of their relative ionic radii.



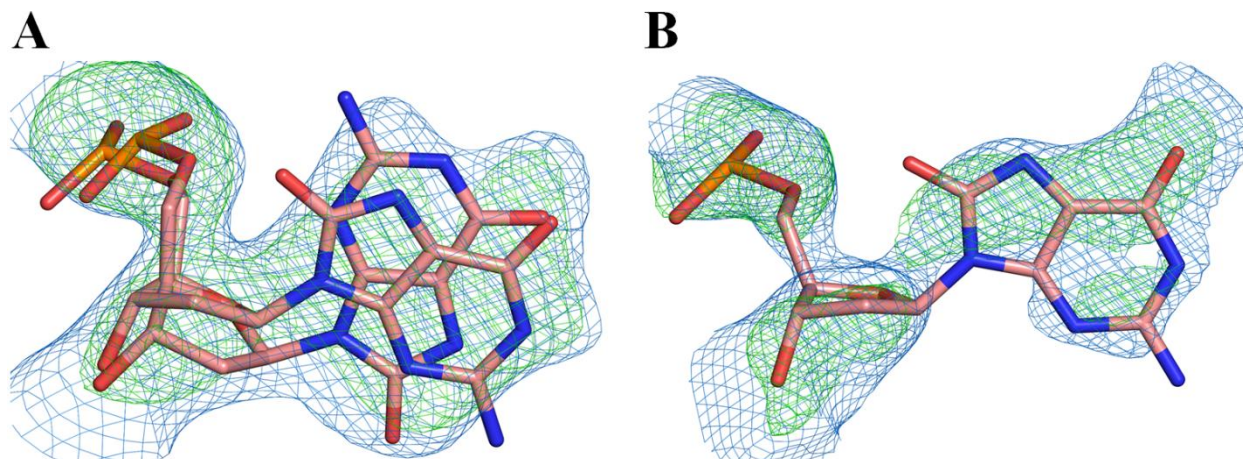


**Figure S6. Electron density maps for the modeling of 8-oxoG conformation in the open binary complex of hPol $\beta$ •8-oxoG-DNA<sub>+1</sub> after 1 hr Mg<sup>2+</sup>/Ca<sup>2+</sup> ion-exchange.** (A) Both *anti*- and *syn*-conformations of the templating nucleotide 8-oxoG were modeled after dCTP incorporation. (B) Only the *anti*-conformation of the templating nucleotide 8-oxoG was modeled after dATP incorporation. For (A) and (B), both 2F<sub>o</sub>-F<sub>c</sub> (blue, 1 $\sigma$ ) and F<sub>o</sub>-F<sub>c</sub> (green, 3 $\sigma$ ) maps are shown.

**Table S1.** Data collection and refinement statistics of the pre-catalytic ternary complex of hPol $\beta$ •8-oxoG-DNA•dCTP after soaking crystals with Mg<sup>2+</sup> for 30 s, 60 s, 80 s and 1 hr, or with Mn<sup>2+</sup> for 35 s.

	Pre-catalytic ternary complex	30 s	60 s	80 s	1 hr	35 s (MnCl <sub>2</sub> )
<b>Data collection*</b>						
Space group	P2 <sub>1</sub>	P2 <sub>1</sub>	P2 <sub>1</sub>	P2 <sub>1</sub>	P2 <sub>1</sub>	P2 <sub>1</sub>
Cell dimension						
<i>a</i> , <i>b</i> , <i>c</i> (Å)	49.6, 79.3, 55.6	49.4, 79.5, 55.5	49.4, 79.3, 55.4	49.6, 79.5, 55.4	55.4, 80.3, 55.8	49.8, 82.2, 54.6
$\alpha$ , $\beta$ , $\gamma$ (°)	90, 106.3, 90	90, 106.6, 90	90, 106.2, 90	90, 106.6, 90	90, 110.2, 90	90, 110.6, 90
Resolution (Å)	31.85-1.90 (1.94-1.90)	31.85-1.90 (1.94-1.90)	44.19-2.19 (2.26-2.19)	47.52-2.20 (2.27-2.20)	52.34-2.70 (2.83-2.70)	46.64-2.20 (2.27-2.20)
<i>R</i> <sub>merge</sub> <sup>†</sup>	0.083 (0.370)	0.092 (0.506)	0.122 (0.548)	0.154 (0.587)	0.079 (0.426)	0.097 (0.604)
<i>I</i> / $\sigma$ <i>I</i>	6.8 (2.0)	7.7 (2.2)	6.4 (2.1)	4.7 (2.1)	8.3 (2.1)	7.7 (2.3)
Completeness (%)	95.4 (91.6)	99.7 (99.8)	97.6 (96.6)	99.3 (99.4)	92.9 (92.5)	90.8 (90.1)
Redundancy	3.3 (3.1)	3.3 (3.2)	3.5 (3.1)	3.2 (3.2)	3.2 (3.0)	3.6 (3.5)
<b>Refinement</b>						
Resolution (Å)	31.43-1.90	31.23-1.90	44.19-2.19	44.18-2.20	45.63-2.70	46.64-2.20
No. reflections	29702	30816	19738	19866	11202	18209
<i>R</i> <sub>work</sub> / <i>R</i> <sub>free</sub> <sup>‡</sup>	0.188/0.226	0.189/0.229	0.195/0.251	0.207/0.268	0.203/0.280	0.194/0.268
<b>No. atoms</b>						
Protein	2641	2636	2627	2628	2598	2692
DNA	633	671	671	652	716	652
Water	246	286	158	126	10	155
<b>B-factors (Å<sup>2</sup>)</b>						
Protein	23.7	21.9	28.0	27.7	62.4	35.9
DNA/dCTP/PPi	25.1/15.9/-	21.5/14.3/15.6	26.5/20.4/28.3	29.1/-/29.3	53.4/-/-	36.9/-/33.6
Water	28.7	29.0	27.8	25.1	33.1	32.9
Metal A/B/C**	18.3/18.7/-	11.3/14.5/17.5	22.4/24.3/25.5	22.1/23.0/30.6	-/-/-	26.3/23.7/35.4
<b>R.m.s deviations</b>						
Bond lengths (Å)	0.006	0.006	0.007	0.007	0.008	0.010
Bond angles (°)	1.283	1.327	1.303	1.320	1.367	1.403
<b>Reaction ratio</b>						
Ratio of RS/PS***	1.0/0.0	0.5/0.5	0.2/0.8	0.0/1.0	0.0/1.0	0.0/1.0
<b>Occupancy</b>						
Metal A/B/C**	1.0/1.0/0	1.0/1.0/0.5	1.0/1.0/0.5	1.0/1.0/1.0	-/-/-	1.0/1.0/0.8
Pyrophosphate	-	0.5	0.8	1.0	-	1.0
<b>PDB ID</b>	4RPX	4RPY	4RPZ	4RQ0	4RQ1	4RQ2

\*Highest resolution shell is shown in parenthesis.

\*\*\* Metal A/B/C refers to the metal ions at the A-, B- and C-site, respectively. Values indicate the occupancy at which the metal ion was modeled in the given structure.

\*\*RS and PS are abbreviations for the reactant state and product state.

<sup>†</sup>*R*<sub>merge</sub> =  $\sum |I - \langle I \rangle| / \sum I$ , where *I* is the integrated intensity of each reflection.

<sup>‡</sup>*R* value =  $\sum (|F_o| - |F_c|) / \sum |F_o|$ , where *F*<sub>o</sub> and *F*<sub>c</sub> are observed and calculated structure factor amplitudes, respectively.

**Table S2.** Data collection and refinement statistics of the pre-catalytic ternary complex of hPol $\beta$ •8-oxoG-DNA•dATP after soaking crystals with Mg<sup>2+</sup> for 30 s, 60 s, 80 s and 1 hr, or with Mn<sup>2+</sup> for 35 s.

	Pre-catalytic ternary complex	30 s	60 s	80 s	1 hr	35 s (MnCl <sub>2</sub> )
<b>Data collection*</b>						
Space group	P2 <sub>1</sub>	P2 <sub>1</sub>	P2 <sub>1</sub>	P2 <sub>1</sub>	P2 <sub>1</sub>	P2 <sub>1</sub>
Cell dimensions						
<i>a</i> , <i>b</i> , <i>c</i> (Å)	49.3, 79.6, 55.4	49.1, 79.6, 55.3	49.2, 79.7, 55.3	50.4, 80.4, 55.6	55.3, 79.6, 55.8	50.2, 82.5, 54.7
$\alpha$ , $\beta$ , $\gamma$ (°)	90, 106.5, 90	90, 106.4, 90	90, 106.6, 90	90, 107.7, 90	90, 109.5, 90	90, 110.8, 90
Resolution (Å)	53.16-2.00 (2.05-2.00)	40.59-2.10 (2.16-2.10)	79.70-2.32 (2.45-2.32)	44.28-2.25 (2.32-2.25)	52.61-2.00 (2.05-2.00)	41.27-2.00 (2.11-2.00)
<i>R</i> <sub>merge</sub> <sup>†</sup>	0.103 (0.472)	0.076 (0.382)	0.081 (0.644)	0.082 (0.542)	0.104 (0.562)	0.120 (0.499)
<i>I</i> / $\sigma$ <i>I</i>	7.3 (2.2)	7.8 (2.5)	11.6 (2.0)	8.7 (2.0)	6.8 (2.2)	5.0 (2.4)
Completeness (%)	95.6 (95.0)	99.7 (99.8)	95.3 (88.2)	98.8 (98.0)	92.7 (90.8)	99.5 (98.7)
Redundancy	3.5 (3.4)	3.2 (3.2)	3.3 (2.7)	3.7 (3.5)	3.6 (3.2)	3.4 (3.2)
<b>Refinement</b>						
Resolution (Å)	47.29-2.00	40.59-2.10	50.0-2.32	44.28-2.25	45.40-2.00	40.79-2.00
No. reflections	25340	22700	16065	18900	27220	26717
<i>R</i> <sub>work</sub> / <i>R</i> <sub>free</sub> <sup>‡</sup>	0.191/0.245	0.189/0.243	0.196/0.265	0.197/0.252	0.206/0.260	0.206/0.270
<b>No. atoms</b>						
Protein	2636	2626	2614	2633	2610	2709
DNA	633	652	652	654	716	654
Water	242	195	77	71	202	231
<b>B-factors (Å<sup>2</sup>)</b>						
Protein	26.7	33.7	38.8	43.3	34.1	27.6
DNA/dCTP/PPi	34.14/25.1/-	40.5/24.6/19.8	44.1/28.8/31.8	51.9/-/34.6	31.3/-/-	32.06/-/23.7
Water	32.7	22.7	29.8	34.7	33.5	30.8
Metal A/B/C <sup>**</sup>	26.6/24.6/-	13.0/19.4/38.2	26.4/27.7/32.7	28.6/28.9/36.7	-/-/-	18.3/17.9/38.7
<b>R.m.s deviations</b>						
Bond lengths (Å)	0.007	0.008	0.009	0.007	0.007	0.009
Bond angles (°)	1.282	1.342	1.413	1.232	1.259	1.359
<b>Reaction ratio</b>						
Ratio of RS/PS <sup>***</sup>	1.0/0.0	0.7/0.3	0.3/0.7	0.0/1.0	0.0/1.0	0.0/1.0
<b>Occupancy</b>						
Metal A/B/C <sup>**</sup>	1.0/1.0/0	1.0/1.0/0.8	1.0/1.0/0.8	1.0/1.0/0.8	-/-/-	1.0/1.0/1.0
Pyrophosphate	-	0.3	0.7	1.0	-	1.0
<b>PDB ID</b>	4RQ3	4RQ4	4RQ5	4RQ6	4RQ7	4RQ8

\*Highest resolution shell is shown in parenthesis.

\*\* Metal A/B/C refers to the metal ions at the A-, B- and C-site, respectively. Values indicate the occupancy at which the metal ion was modeled in the given structure.

\*\*\*RS and PS are abbreviations for the reactant state and product state.

<sup>†</sup>*R*<sub>merge</sub> =  $\sum |I - \langle I \rangle| / \sum I$ , where *I* is the integrated intensity of each reflection.

<sup>‡</sup>*R* value =  $\sum (|F_o| - |F_c|) / \sum |F_o|$ , where *F*<sub>o</sub> and *F*<sub>c</sub> are observed and calculated structure factor amplitudes, respectively.

**Table S3.** Coordinating ligands for each metal-ion site during dCTP or dATP incorporation. The table lists the identity of the ligands coordinating each metal ion, *e.g.* the primer 3'-OH (3'-OH), pyrophosphate (PPi), water molecule (W), and the oxygen atoms of the phosphate groups of bound dCTP/dATP or incorporated dCMP/dAMP, and their coordination numbers in parentheses.

	<b>Metal Ion</b>	<b>50% Incorporation (Mg<sup>2+</sup> soak)</b>	<b>80% Incorporation (Mg<sup>2+</sup> soak)</b>	<b>100% Incorporation (Mg<sup>2+</sup> soak)</b>	<b>100% Incorporation (Mn<sup>2+</sup> soak)</b>
<b>dCTP</b>	<b>A-site</b>	Mg <sup>2+</sup> : D256 (1), D192 (1), D190 (1), 3'-OH (1), dCTP/dCMP (1), W (1)	Mg <sup>2+</sup> : D256 (1), D192 (1), D190 (1), 3'-OH (1), dCTP/dCMP (1)	Na <sup>+</sup> : D256 (1), D192 (1), D190 (1), 3'-OH (1), dCMP (1),	Mn <sup>2+</sup> : D256 (1), D192 (1), D190 (1), 3'-OH (1), dCMP (1), W (1)
	<b>B-site</b>	Mg <sup>2+</sup> : D192 (1), D190 (1), dCTP/dCMP (1), PPi (2), W (1)	Mg <sup>2+</sup> : D192 (1), D190 (1), dCTP/dCMP (1), PPi (2), W (1)	Mg <sup>2+</sup> : D192 (1), D190 (1), dCMP (1), PPi (2), W (1)	Mn <sup>2+</sup> : D192 (1), D190 (1), dCMP (1), PPi (2), W (1)
	<b>C-site</b>	Mg <sup>2+</sup> : dCTP/dCMP (1), PPi (1), W (4)	Mg <sup>2+</sup> : dCTP/dCMP (1), PPi (1), W (4)	Mg <sup>2+</sup> : dCMP (1), PPi (1), W (4)	Mn <sup>2+</sup> : dCMP (1), PPi (1), W (4)
<b>dATP</b>	<b>Metal Ion</b>	<b>30% Incorporation (Mg<sup>2+</sup> soak)</b>	<b>70% Incorporation (Mg<sup>2+</sup> soak)</b>	<b>100% Incorporation (Mg<sup>2+</sup> soak)</b>	<b>100% Incorporation (Mn<sup>2+</sup> soak)</b>
	<b>A-site</b>	Mg <sup>2+</sup> : D256 (1), D192 (1), D190 (1), 3'-OH (1), dAMP /dATP (1), W (1)	Mg <sup>2+</sup> : D256 (1), D192 (1), D190 (1), 3'-OH (1), dATP/dAMP (1), W (1)	Na <sup>+</sup> : D256 (1), D192 (1), D190 (1), 3'-OH (1), dAMP (1))	Mn <sup>2+</sup> : D256 (1), D192 (1), D190 (1), 3'-OH (1), dAMP (1), W (1)
	<b>B-site</b>	Mg <sup>2+</sup> : D192 (1), D190 (1), dATP/dAMP (1), PPi (2), W (1)	Mg <sup>2+</sup> : D192 (1), D190 (1), dATP/dAMP (1), PPi (2), W (1)	Mg <sup>2+</sup> : D192 (1), D190 (1), dAMP (1), PPi (2), W (1)	Mn <sup>2+</sup> : D192 (1), D190 (1), dAMP (1), PPi (2), W (1)
	<b>C-site</b>	Mg <sup>2+</sup> : dATP/dAMP (1), PPi (1), W (3)	Mg <sup>2+</sup> : dATP/dAMP (1), PPi (1), W (2)	Mg <sup>2+</sup> : dAMP (1), PPi (1), W (4)	Mn <sup>2+</sup> : dAMP (1), PPi (1), W (3)